COBEM 2023 27TH INTERNATIONAL CONGRESS OF MECHANICAL ENGENEERING

ABCM Brazilian Society of Mechanical Sciences and Engineering
27th ABCM International Congress of Mechanical Engineering
December 04-08, 2023, Florianópolis-SC, Brazil

COB-2023-0389
NUMERICAL ANALYSIS OF DIFFERENT CONFIGURATIONS OF A COMPLEX COMMERCIAL SINK SUBJECTED TO FORCED CONVECTIVE TURBULENT FLOWS

Tarciso Melo Claudino[a]
Otávio Franz Zauk[b]
Liércio André Isoldi[c]
School of Engineering, Universidade Federal do Rio Grande – FURG, Av. Itália, km 8, Rio Grande, RS, 96203-900, Brazil.
[a] tarcisoclaudino@furg.br
[b] otaviozauk@gmail.com
[c] liercioisoldi@furg.br

Luiz Alberto Oliveira Rocha
Department of Mechanical Engineering, Universidade Federal do Rio Grande do Sul - UFRGS, Rua Sarmento Leite, 425, Porto Alegre, RS, 90050-170, Brazil.
luizrocha@mecanica.ufrgs.br

Paulo Lilles Jorge Drews Junior
Computational Sciences Center, Universidade Federal do Rio Grande - FURG, Av Itália, km 8, Rio Grande, RS, 96203-900, Brazil.
paulodrews@furg.br

Elizaldo Domingues dos Santos
School of Engineering, Universidade Federal do Rio Grande - FURG, Av Itália, km 8, Rio Grande, RS, 96203-900, Brazil.
elizaldosantos@furg.br

Abstract. *The compactness of electronic packaging embarked in autonomous drones associated with the increase of processing capacities of the electronic compounds has increasing their heat generation per unit volume. Moreover, the control of temperature is a chief aspect to ensure the life cycle of the electronic packaging of the drone. The present work has the purpose to perform a numerical investigation of a commercial heat sink with complex configuration subjected to turbulent, incompressible, three-dimensional, and forced convective flow. Different geometric configurations are investigated seeking to obtain a theoretical recommendation about the influence of the geometry over the heat transfer rate between a commercial sink (NVIDIA Jetson Nano™) and the turbulent forced convective flow. The sink simulated is used for cooling the electronic components of a microcomputer used in autonomous unmanned aerial vehicle (UAV). More precisely, it was investigated four different configurations of one fin of the sink with different positions (defined by the ratio between the distance of intermediate fin to the center of sink and the total length of the sink, L_1/L) and different inclination angles of the fin to the horizontal axis (α_1). The four proposed studied cases have the following configurations: Case 1: L_1/L = 0.0705 and α_1 = 50º; Case 2: L_1/L = 0.167 and α_1 = 96º; Case 3: L_1/L = 0.2635 and α_1 = 105º; Case 4: L_1/L = 0.363 and α_1 = 115º. The results of heat transfer rate between the heat sink and the fresh surrounding flow obtained for the four cases were compared with the original configuration of the commercial sink (Case 5: L_1/L = 0.222 and α_1 = 80º). For the prediction of fluid dynamic and thermal fields, time-averaged conservation equation of mass, balance of momentum, and conservation of energy were solved with the Finite Volume Method (FVM), more precisely with the commercial code FLUENT (Version 2021 R1). For closure of time-averaged equations, it was used the Reynolds Averaged Navier Stokes (RANS) k – ω SST (Shear Stress Transport) model. It was considered for all simulated cases a turbulent forced convective flow with Reynolds and Prandtl numbers of Re_L = 53,000 and P_r = 0.71. Results indicated a difference of nearly 9.0 % in heat transfer rate when the best and the worst configurations were compared. Moreover, the best configuration led to a performance 6.4% superior to the original configuration of the sink, showing that the original configuration of the heat sink can have its design improved.*

Keywords: *Numerical simulation, Forced Convective Turbulent Flows, Complex Heat Sink, Geometric Investigation*

1 INTRODUCTION

Unmanned aerial vehicle (UAV) represents an important technological achievement in several fields as in the remote sensing, foliar fertilizers in agriculture, capturing of images for digital media, maintenance of engineering systems, and even for armed forces security. Therefore, the development of technological research to improve the UAV performance

is an important subject (Yao *et al.*, 2019). Despite of recent achievements, the technological advancement of drones still faces some hindrances. For example, the cooling of electronic packaging embarked in the drones is a challenging task since the processing power per unit volume is increasing dramatically. For small size drones, the airflow surrounding the drone has been used for the cooling of the embarked microcomputers.

One of the main motivations of the present work is related to the development of an autonomous drone in the project *Hydrone* by the Computational Sciences Center (C3) of the Federal University of Rio Grande (FURG) (Drews *et al.*, 2014). This drone uses a platform composed of four rotors to control its movement. The device also has a microcomputer that control its movement and executes several neural networks in parallel to perform the classification of images and detection of objects. Figure 1 illustrates the drone sketch, Fig. 1(a), and the device in operation during one competition named *Robótica* in 2019, Fig. 1(b). For the rotor system used, the imbalance caused by different velocities imposed at the rotors generates the movement of the device in a stable and maneuverable way, leading to advantages as locomotion in low altitudes and stability, even under the action of the gravity forcing the device towards the soil. However, the employment of the four rotors and the perturbations imposed by the wind over the device, especially in external environments, has led to an increase of processing operations in the microcomputer and, consequently, in the energy consumption of the device (Horn, 2019; Grando *et al.*, 2020).

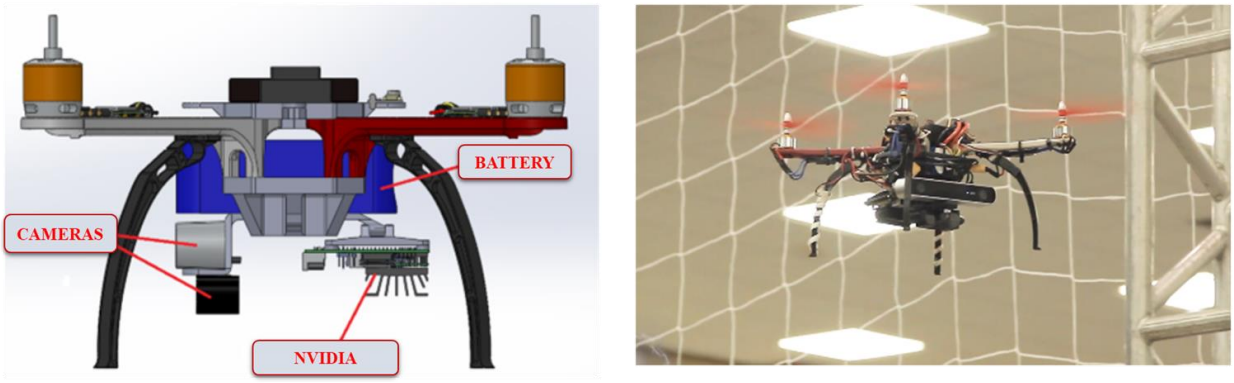

Figure 1. Illustration of the studied device: a) drone project (*Hydrone*); b) drone in operation in *Robótica* event.

Figure 2 illustrates the sink used in the processor of *NVIDIA® Jetson Nano™*, installed in the microcomputer of the drone. During the operation of the UAV, it was noted that the microcomputer operates at a mean temperature near the shutdown temperature for protection of the processor ($T_s \sim 100$ °C), generating several problems as communication losses in the vision system of the drone and, even, operation interruption. In the latter condition, a catastrophic failure can occur as physical device crash and physical or material damage to third parties. In this sense, the microcomputer is placed in a region where the airflow has the highest possible magnitude. Despite that, the initial project of the drone does not take into account other strategies for the microcomputer cooling, and it is still facing difficulties on the operation due to the overheating of electronic packaging.

Figure 2. Illustration of sink used in the NVIDIA® Jetson Nano™ Processor.

Literature has reported the use of several strategies for cooling of heat generating energy systems as the use of heat pipes (where a liquid fluid or a fluid in phase change dissipates the heat from the electronic package), plate heat exchangers, thermal paste, Peltier devices, use of micro-channel heat exchangers with several configurations, and the use

of heat sinks under forced or free convective flows (Niqiuddin et al., 2018; Chung and Kim, 2019). The present work focused on the use of the strategy commonly adopted for cooling of electronic packaging of small sized UAVs, i.e., the cooling by means of convection of airflow passing over the heated sink of the processor. This strategy was chosen in a first moment since it does not require additional system work for pumping a cooling flow embarked in the drone. More precisely, it was performed here a numerical investigation about the influence of the geometrical configuration of the fins of sink used in the *NVIDIA® Jetson Nano™* processor over the heat transfer rate between the heated sink and the surrounding forced convective turbulent flow. The main purposes here were to develop a computational model that represents the forced convective turbulent flow over a complex configuration of processor sink and evaluate if changes in the sink design can led to improvements in the system thermal performance. In this sense, four different configurations were investigated and compared with the commercial configuration of the system. For all geometrical configurations, the maximum volume occupied by the complex sink and the heat transfer area between the sink and the surrounding flow were kept constant. This work is based on the proof of concept, i.e., if the investigated configurations improved the system thermal performance, a geometrical optimization can be proposed as a possible solution to mitigate the overheating of the electronic compounds of the microcomputer of the investigated drone.

2 MATHEMATICAL MODELING

In the present work, it was considered a conjugate convection/conduction heat transfer problem. The following considerations for the convective heat transfer were assumed: the airflow is incompressible, turbulent, the domain is three-dimensional, the thermophysical properties are constant and the driven is caused by forced convection (mimicking the relative difference of velocity between the drone and the environment in one specific condition). For closure of turbulence modeling, it is adopted the $k-\omega$ SST (Shear Stress Transport) model. The thermal field in the sink (made of aluminum) is also solved considering constant thermophysical properties. Moreover, the sink material is not under effect of heat generation. For the conjugated convective-conductive problem it is considered that the solution is performed in transient regime, while the analysis is performed when the flow reaches the steady state.

For the modeling of turbulent air flow over the heated sink, it is solved the time-averaged conservation equation of mass, momentum in *x*, *y*, and *z* directions, and conservation of energy, which are given by (Pope, 2008; Wilcox, 2006; Bejan, 2013):

$$\frac{\partial \bar{u}}{\partial x}+\frac{\partial \bar{v}}{\partial y}+\frac{\partial \bar{w}}{\partial y}=0 \tag{1}$$

$$\rho\left(\frac{\partial \bar{u}}{\partial t}+\bar{u}\frac{\partial \bar{u}}{\partial x}+\bar{v}\frac{\partial \bar{u}}{\partial y}+\bar{w}\frac{\partial \bar{u}}{\partial z}\right)=-\frac{\partial \bar{p}}{\partial x}+(\mu+\mu_t)\left(\frac{\partial^2 \bar{u}}{\partial x^2}+\frac{\partial^2 \bar{u}}{\partial y^2}+\frac{\partial^2 \bar{u}}{\partial z^2}\right) \tag{2}$$

$$\rho\left(\frac{\partial \bar{v}}{\partial t}+\bar{u}\frac{\partial \bar{v}}{\partial x}+\bar{v}\frac{\partial \bar{v}}{\partial y}+\bar{w}\frac{\partial \bar{v}}{\partial z}\right)=-\frac{\partial \bar{p}}{\partial y}+(\mu+\mu_t)\left(\frac{\partial^2 \bar{v}}{\partial x^2}+\frac{\partial^2 \bar{v}}{\partial y^2}+\frac{\partial^2 \bar{v}}{\partial z^2}\right) \tag{3}$$

$$\rho\left(\frac{\partial \bar{w}}{\partial t}+\bar{u}\frac{\partial \bar{w}}{\partial x}+\bar{v}\frac{\partial \bar{w}}{\partial y}+\bar{w}\frac{\partial \bar{w}}{\partial z}\right)=-\frac{\partial \bar{p}}{\partial z}+(\mu+\mu_t)\left(\frac{\partial^2 \bar{w}}{\partial x^2}+\frac{\partial^2 \bar{w}}{\partial y^2}+\frac{\partial^2 \bar{w}}{\partial z^2}\right) \tag{4}$$

$$\rho C_P\left(\frac{\partial \bar{T}}{\partial t}+\bar{u}\frac{\partial \bar{T}}{\partial x}+\bar{v}\frac{\partial \bar{T}}{\partial y}+\bar{w}\frac{\partial \bar{T}}{\partial z}\right)=(k+k_t)\left(\frac{\partial^2 \bar{T}}{\partial x^2}+\frac{\partial^2 \bar{T}}{\partial y^2}+\frac{\partial^2 \bar{T}}{\partial z^2}\right) \tag{5}$$

The equations for turbulent viscosity and thermal diffusivity, are given by (Menter *et al.*, 2003):

$$\mu_t=\frac{\rho\alpha_1\kappa}{max(\alpha_1\omega, SF_2)} \tag{6}$$

$$\alpha_t=\frac{k_t}{\rho C_P}=\frac{\mu_t}{\rho Pr_t} \tag{7}$$

In Eqs. (1) - (7), (¯) represents the time-average operator, *x*, *y*, and *z* represent the spatial coordinates (m), *u*, *v*, and *w* are the velocities in *x*, *y*, and *z* directions (m/s), respectively; ρ is the density (kg/m³); *t* is the time (s); *p* is the pressure (Pa); μ is the dynamic viscosity (kg/m·s); μ_t is the turbulent viscosity (kg/m·s); *T* is the temperature (K); α is the thermal diffusivity (m²/s), given by $k/(\rho cp)$; *k* is the thermal conductivity of the air (W/(m·K); c_p is the specific heat capacity (J/kg K); α_t is the turbulent thermal diffusivity (m²/s); κ is the turbulent kinetic energy (m²/s²); ω is the specific dissipation rate (1/s); Pr_t is the turbulent Prandtl number, given by υ_t/α_t; υ_t is the turbulent kinetic viscosity, μ_t/ρ (m²/s).

The turbulent kinetic energy (κ) and the specific dissipation rate (ω) are given by:

$$\frac{\partial \kappa}{\partial t} + \bar{u}_i \frac{\partial \kappa}{\partial x_i} = \widetilde{P_\kappa} - \frac{\kappa^{\frac{1}{2}}}{L_T} + \frac{\partial}{\partial x_i}\left[\left(\mu + \sigma_{\kappa\mu_t}\right)\frac{\partial \kappa}{\partial x_i}\right] \tag{8}$$

$$\frac{\partial \omega}{\partial t} + \bar{u}_i \frac{\partial \kappa}{\partial x_i} = \left(\frac{\alpha}{\mu_t}\right)\widetilde{P_\kappa} - \beta^* \omega^2 + \left[\left(\mu + \sigma_{\omega\mu_t}\right)\frac{\partial \omega}{\partial x_j}\right] + 2(1 - F_1)\frac{\sigma\omega^2}{\omega}\frac{\partial \kappa}{\partial x_i}\frac{\partial \omega}{\partial x_i} \tag{9}$$

where *i* = 1, 2, and 3 represent the spatial coordinates in *x*, *y*, and *z* directions; $\widetilde{P_\kappa}$ is a function that prevents the turbulence generation in stagnation regions; β = 0.09, α_1 = 5/9, β_1 = 3/40, σ_k = 0.85, σ_w = 0.5, σ_2 = 0.44, β_2 = 0.0828, σ_{k2} = 1, and σ_{w2} = 0.856 are ad hoc constants used in Menter (1993) and F_1 and F_2 are blending functions between variables, and are defined by:

$$F_1 = tanh\left\{\left\{min\left[max\left(\frac{\kappa^{1/2}}{\beta^*\omega y}, \frac{500\upsilon}{y^2\omega}\right), \frac{4\rho\sigma_{\omega 2}\kappa}{CD_{k\omega}y^2}\right]\right\}^4\right\} \tag{9}$$

$$F_2 = tanh\left\{\left[max\left(\frac{2\kappa^{1/2}}{\beta^*\omega y}, \frac{500\upsilon}{y^2\omega}\right)\right]^2\right\} \tag{10}$$

In the thermal sink, the heat diffusion equation is solved for definition of temperature field in the solid domain. The energy equation in this region is given by (Han and Özisik, 1993):

$$\rho_s C_{P,s}\frac{\partial T_s}{\partial t} = k_s\left(\frac{\partial^2 T_s}{\partial x^2} + \frac{\partial^2 T_s}{\partial y^2} + \frac{\partial^2 T_s}{\partial z^2}\right) \tag{11}$$

where T_s is the temperature in the solid domain (K); ρ_s is the solid density (kg/m³); $C_{P,s}$ is the specific heat capacity of the solid (J/kg·K); and k_s is the thermal conductivity of the solid (W/m·K).

3. PROBLEM DESCRIPTION

The heat transfer problem studied here consists of a channel where the air flows through the thermal sink mounted in the lower surface of the channel, as illustrated in Fig. 3. Figure 3(a) shows the domain in perspective with the inlet of the turbulent airflow (green surface), outlet of heated airflow after passing through the heated sink (red surface), and the sink (solid domain). The fluid flow is caused by the imposition of a constant velocity at the inlet surface of the domain with V_{in} = 3.0 m/s, turbulence intensity of *I* = 3.0 %, and with a constant temperature of T_{in} = 293.15 K. The heat transfer occurs due to the difference of temperature between the entering airflow in the channel (T_{in}) and the temperature imposed in the basis of the sink (inferior face of the sink) which is T_S = 370.15 K. This temperature simulates the heating caused by the electronic compounds connected to the heat sink in an extreme condition near the shutdown of the electronic package. Concerning the other boundary conditions, the outlet surface, red surface in Fig. 3(a), has a null pressure gauge (p_g = 0 atm), while the surfaces of the sink as well as the channel surfaces has no-slip and impermeability boundary conditions ($u = v = w$ = 0 m/s). The channel surfaces are also thermally insulated (q'' = 0 W/m²). Figure 3(b) illustrates the domain of the heat sink with rounded surface in comparison with the real domain (see Fig. 2). Figures 3(c) and 3(d) illustrate the frontal and lateral views of the channel with the heat sink mounted in the lower surface of the channel. It is also presented the dimensions of the computational domain where *L* = 20 mm. For all cases, it is considered a constant Reynolds number ($Re_H = \rho V_{in} H/\mu$ = 53,000) and Prandtl number ($Pr = \upsilon/\alpha$ = 0.74). The thermophysical properties of air and aluminum are seen in Table 1.

Table 1. Thermophysical properties of the air and aluminum in the studied problem.

Properties / Material	Air	Aluminum
Density (kg/m³)	1.225	2719.0
Specific heat capacity (J/kg.K)	1006.43	871.0
Thermal conductivity (W/mK)	24.2×10^{-3}	202.4
Dynamic viscosity (kg/ms)	1.79×10^{-5}	

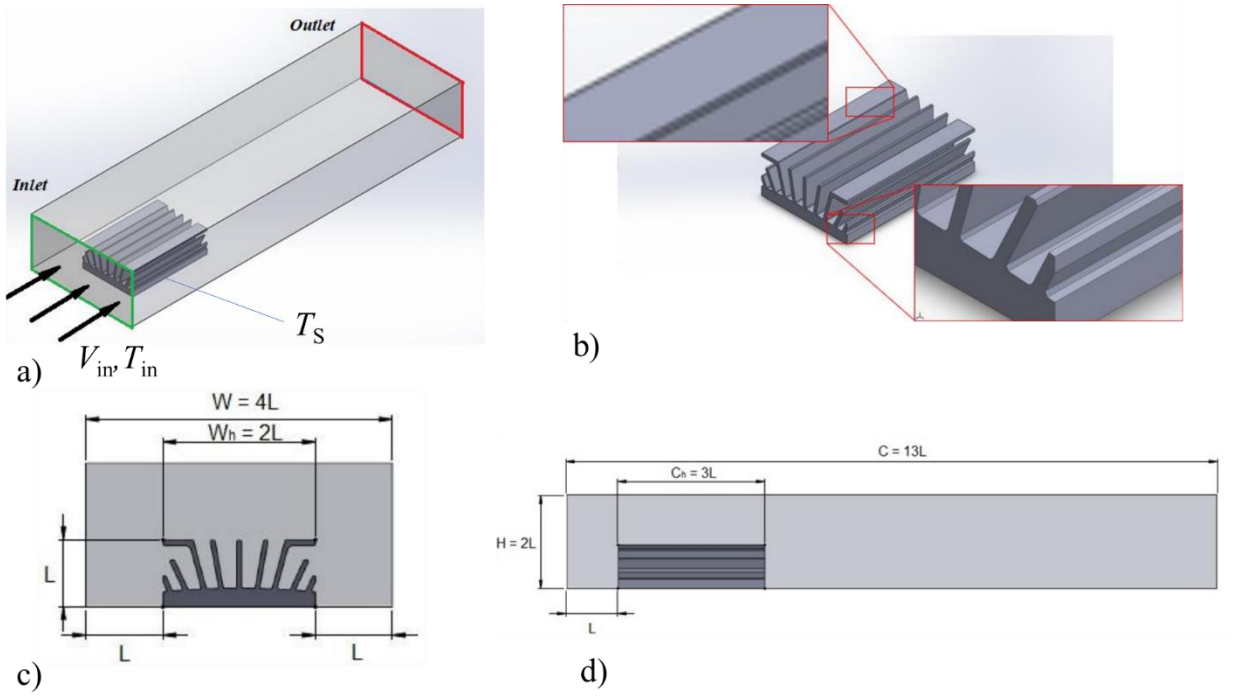

Figure 3. Illustration of the computational domain: a) isometric perspective, b) detail of the thermal sink, c) frontal view of the channel with the sink and dimensions, d) lateral view of the channel with the sink and dimensions.

In the present study, five different configurations are simulated in order to have an initial idea whether the fins configuration can affect the performance of the heat sink and the geometrical optimization can be a possible strategy to mitigate the overheating of the electronic package of the microcomputer embarked in the drone. Figure 4 illustrates the heat sink with all possible degrees of freedom to be investigated, i.e., the sink can have up to 8 degrees of freedom: L_1/L, L_2/L, L_3/L, L_4/L, α_1, α_2, α_3, α_4. If six different magnitudes were investigated for each degree of freedom, it would be required more than 46,000 simulations to explore all geometric combinations, making the investigation unviable for the present conditions. Despite that, the design of heat sink is a strategy to be investigated. Then, here it is performed an exploration where five different cases are simulated giving an initial idea about the influence of the geometric configuration of the fins over the system thermal performance. Here, five different cases are simulated and the degrees of freedom L_1/L and α_1 used in each simulation are described in Table 2. The other dimensions are kept constant for all investigated cases. The configurations proposed here where the best configurations found in a preliminary investigation with 16 configurations simulated in a laminar flow. The other configurations of L_1/L and α_1, as well as, other dimensions can be explored in the future if the present results indicate some influence of geometry over the thermal performance of the system. It can also be observed in Fig. 4 that all geometric variations must respect an occupation area given by A_0.

Table 2. Geometric configurations investigated in the different studied cases simulated in the present work.

Case / Degree of freedom	L_1/L	α_1
Case 1	0.0705	50º
Case 2	0.1670	96º
Case 3	0.2635	105º
Case 4	0.3630	115º
Case 5 (original configuration)	0.2225	80º

In order to define some limits of geometrical investigation, it is defined a lowest and highest magnitudes of L_1 in order to prevent the interaction with the adjacent fin, placed at L_2 from the central portion of the sink, as illustrated in Fig. 5(a). The distances L_1 investigated are also illustrated in Fig. 5(a). A similar procedure was adopted for the fin inclination α_1.

For example, Fig. 5(b) illustrates the minimum and maximum angles that can be obtained for the case with L_1 = 3.34 mm (L_1/L = 0.1670).

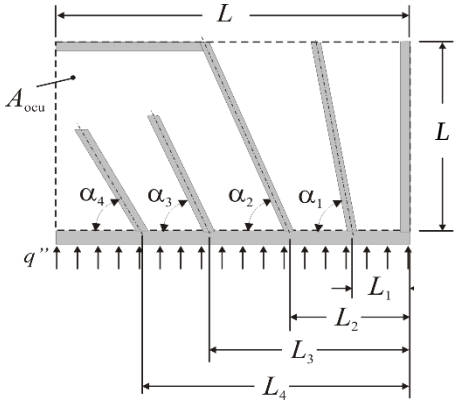

Figure 4. Illustration of half of the domain of the heat sink with the degrees of freedom that can be investigated to improve the thermal performance of the system.

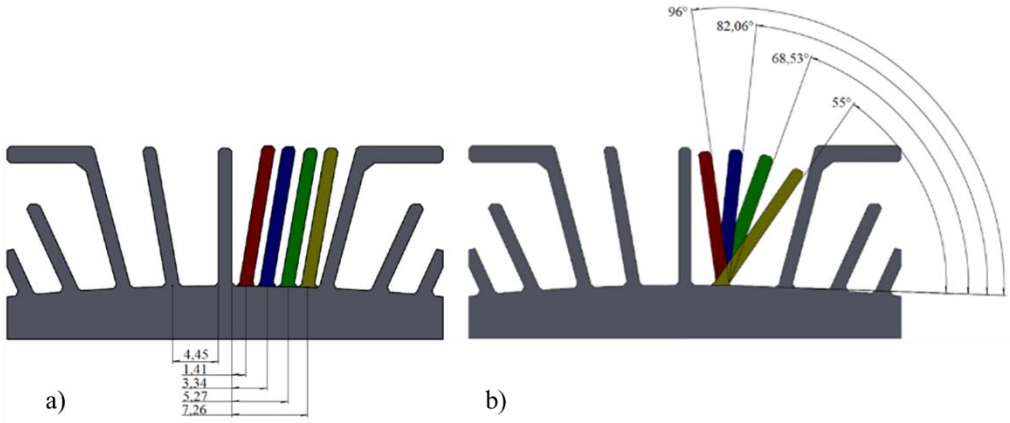

Figure 5. Illustration of the limits imposed on the fin variation in the present problem: a) distance L_1, b) angle α_1 for a specific ratio of L_1/L (magnitudes of L_1 in mm).

4. NUMERICAL MODELING

The equations that model the present problem, Eqs. (1) – (11), are solved numerically with the Finite Volume Method (FVM) implemented in the software FLUENT, version 2022 R1 (Patankar, 1980; Versteeg and Malalasekera, 2007; Maliska, 2004; ANSYS, 2021). Concerning the numerical procedures, it is used the method SIMPLEC (semi-implicit method for pressure-linked equations – consistent) which is a variation of the SIMPLE method (semi-implicit method for pressure-linked equations) developed by Patankar and Spalding (1972). For the treatment of advective terms, the second-order upwind interpolation function is used for the equations of momentum and energy, while the first-order upwind scheme is applied for the equations of transport of turbulent kinetic energy (κ) and specific dissipation rate (ω). The convergence for the simulations is achieved when, for each time step, the residuals of convergence are lower than $R_{esid} \leq 1.0 \times 10^{-6}$ between two successive iterations.

The sink domain, as illustrated in Fig. 6(a), has a refined mesh using prismatic volumes near the boundary between the heat sink and the surrounding fluid region with the intention to capture the velocity and temperature gradients in a more properly form. Moreover, the refinement was performed in such way the $y^+ = yu_\tau/\upsilon \leq 1.0$ to guarantee the correct prediction of turbulent boundary layer, being u_τ the friction velocity – $u_\tau = (\tau_w/\rho)^{1/2}$. On the other hand, the fluid domain, see Fig. 6(b), has a region far from the sink where the mesh is coarser and composed of tetrahedral volumes. In Figure 6(c) it can be noticed the lower surface of the channel with the refinement of the mesh near the heat sink. The employed grid for every simulated case is composed of nearly 700,000 hybrid prismatic and tetrahedral finite volumes.

For transient solution, it is used a time step $\Delta t = 1.0 \times 10^{-3}$ s, and a final time of t = 4.0 s of simulation, being the interval between 3.0 s $\leq t \leq$ 4.0 s used for time averaged parameters. The computational effort for each simulation in a computer with an Intel i5 processor with 2.80 GHz overclocking and 16 GB of RAM memory is nearly 5 h.

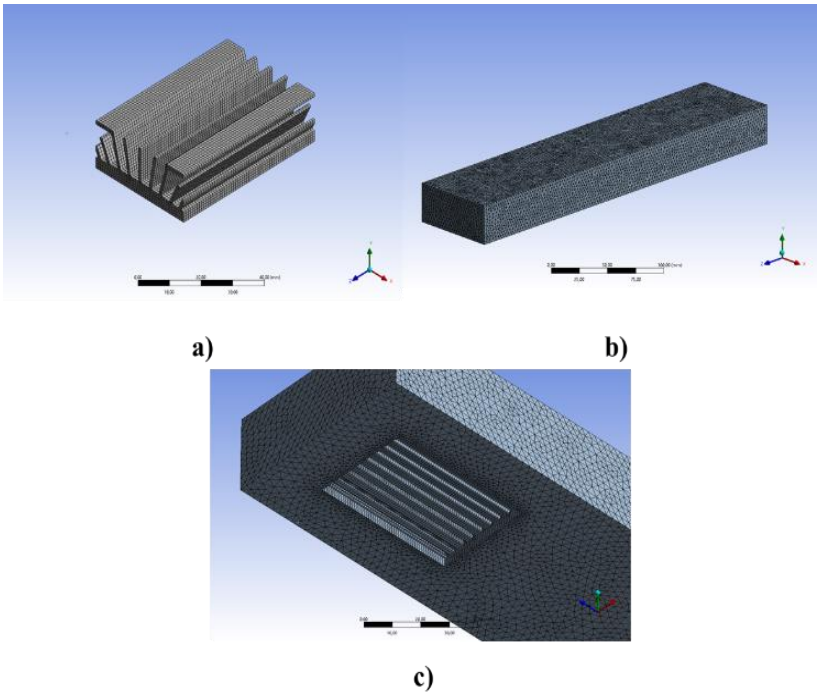

Figure 6. Mesh employed in the present study cases: a) prismatic mesh used in the heat sink; b) view of the general grid generated in the channel; c) view of the inferior surface of the channel with refinement of the grid near the heat sink.

5. RESULTS AND DISCUSSION

Before to perform the investigation of the sink with different geometries subjected to turbulent forced convective flows, two study cases were performed with the aim to verify/validate the present computational method. In the first case, a rectangular fin subjected to constant convective heat transfer is simulated to investigate the prediction of thermal field in the solid domain of the present problem. The numerical simulation results obtained with the present code were compared with an analytical solution of this problem available in Incropera Figure 7(a) shows the domain of the problem with the boundary conditions (h = 100 W/(m²K), T_S = 370.15 K, and T_∞ = 293.15 K) and Fig. 7(b) shows the temperature field along the coordinate x predicted numerically and the analytical solution. The analysis of temperature field distribution revealed a very good agreement between the numerical and analytical predictions, with a difference of nearly 0.2 %. Therefore, it is possible to affirm that the present computational method was verified to solve thermal field in the solid domain.

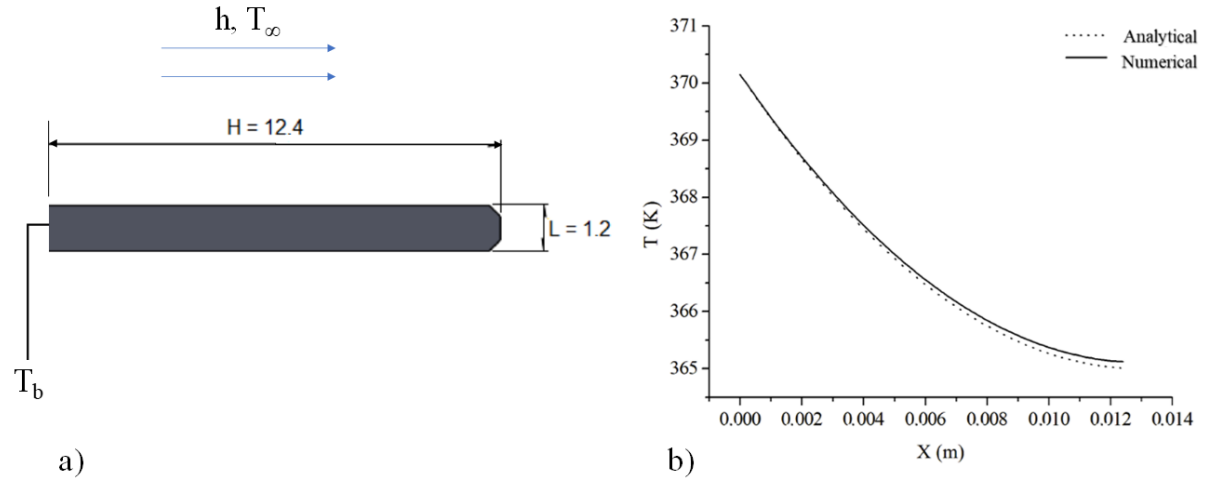

Figure 7. Verification of the computational code for prediction of thermal field in the solid domain of a fin: a) computational domain simulated, and b) comparison between numerical and analytical solutions for the thermal field along the coordinate x.

For the simulation of shear flows under forced convective turbulent flows, which is a similar base flow than that studied here, the present computational method was used for simulation of a case of turbulent flow over a square bluff body with Re_D = 22,000 and Pr = 0.71. This case was previously simulated in the work of Teixeira *et al.* (2018), therefore the computational domain and thermal conditions can be seen in this work. Table 3 shows the time and spatial averaged Nusselt number obtained with the present code and the results predicted by correlation of Hilpert (1933), experimental work of Igarashi (1985), and computational model of Ranjan and Dewan (2015). Results indicated that the predictions reached with the present work are in good agreement, mainly with the experimental work of Igarashi (1985) where a difference of 2.5 % was achieved. Therefore, the present model is considered validated for the simulations of turbulent convective flows over heat sink mounted in the channel.

Table 3. Comparison of time and spatial averaged Nusselt number obtained for turbulent forced convective flow over a bluff body (Re_D = 22,000 and Pr = 0.71)

Source	**Nusselt number ($\overline{Nu}_D$)**	**Relative difference (%)**
Hilpert (1933)	115.8	9.4 %
Igarashi (1985)	107.6	2.5 %
Ranjan and Dewan (2015)	100.4	4.5 %
Present work	104.9	------

Figure 8 shows the heat transfer rate obtained between the heat sink and the turbulent forced convective flow for the five studied geometric configurations. The studied cases were defined from preliminary tests performed in the work of Zauk (2022) with laminar flow (Re_H = 100) where two degrees of freedom (L_1/L and α_1) were investigated subjected to two constraints (volumes of the heat sink and its occupation) following the constructal design method (Bejan, 2000; Dos Santos et al., 2017). It is assumed that, if important differences are reached for the selected cases, the investigation with constructal design can be repeated for the forced convective turbulent flows. It is also illustrated the thermal fields around the heat sink for the different geometries investigated. It was observed that Case 3 (L_1/L = 0.363 and α_1 = 115º) led to the best thermal performance, with q = 64.01 W. For this configuration, the basis of the varied fin is placed near the second fin and the top position of the fins is placed near the central fin, i.e., inclined contrarily than the commercial configuration. The Case 4 performed nearly 6.0 % better than the original commercial configuration (L_1/L = 0.2225 and α_1 = 80°) and nearly 8.0 % superior to the worst configuration, obtained for Case 2 (L_1/L = 0.167 and α_1 = 96°). The best configuration was achieved when the thermal field is distributed in a most homogeneous form and the worst performance is reached when the fins are mounted near each other, preventing the heat exchange in some surfaces of the fins, as seen in thermal field of Case 2. Peripheral fins also has a sort of temperature concentration due to proximity of the fins and can be improved in a future investigation. Even the differences found was not so elevated, only two degrees of freedom (L_1/L and α_1) were analyzed. Therefore, geometric investigation in this problem seems promising as an alternative to mitigate the overheating of the electronic packaging used in the drone. Moreover, the design proposed in the commercial configuration has potential to be improved.

6. CONCLUSIONS

The present numerical work performed the development of a computational approach for investigation of the heat sink used in a microcomputer embarked in an autonomous drone. Moreover, a comparison of different geometrical configurations of heat sink subjected to turbulent, forced convection flows of air in a three-dimensional channel was performed, simulating the conditions that the device is subjected when operating in the unmanned aerial vehicle (UAV). More precisely, five different cases where investigated: Case 1: L_1/L = 0.0705 and α_1 = 50º; Case 2: L_1/L = 0.167 and α_1 = 96º; Case 3: L_1/L = 0.2635 and α_1 = 105º; Case 4: L_1/L = 0.363 and α_1 = 115º; and Case 5: L_1/L = 0.2225 and α_1 = 80º, which represents the original commercial configuration. For all cases, it was considered convective flows with Reynolds and Prandtl numbers of Re_D = 53,000 and Pr = 0.71. For the prediction of fluid dynamic and thermal fields, time-averaged conservation equation of mass, balance of momentum, and conservation of energy were solved with the Finite Volume Method (FVM), implemented in the FLUENT code (Version 2021 R1).

Firstly, two separated cases were simulated for verification and validation of the prediction of thermal field in the solid domain and prediction of turbulent free shear flow over a bluff body. The results obtained with the code for thermal field and time and spatial averaged Nusselt number had good agreement with previous predictions presented in the literature. Concerning the geometrical investigation of the heat sinks, the best configuration (Case 4) performed nearly 9.0 % and 6.0 % better than the worst configuration (Case 2) and commercial configuration (Case 5). Even the differences were not significant, the results obtained in the present work demonstrated that the geometrical investigation can be a promising strategy to mitigate the overheating of electronic packaging in the microcomputer embarked in the drone, especially by the fact that only two of eight degrees of freedom were analyzed. Moreover, results indicated that a homogeneous distribution of the fins, in order to prevent the interaction of thermal boundary layers of the fins, led to the

best thermal performance. In this sense, the best configuration has a fins distribution dissimilar to that constructed for the commercial configuration.

For future studies, it is recommended the investigation of other degrees of freedom and using other thermal conditions.

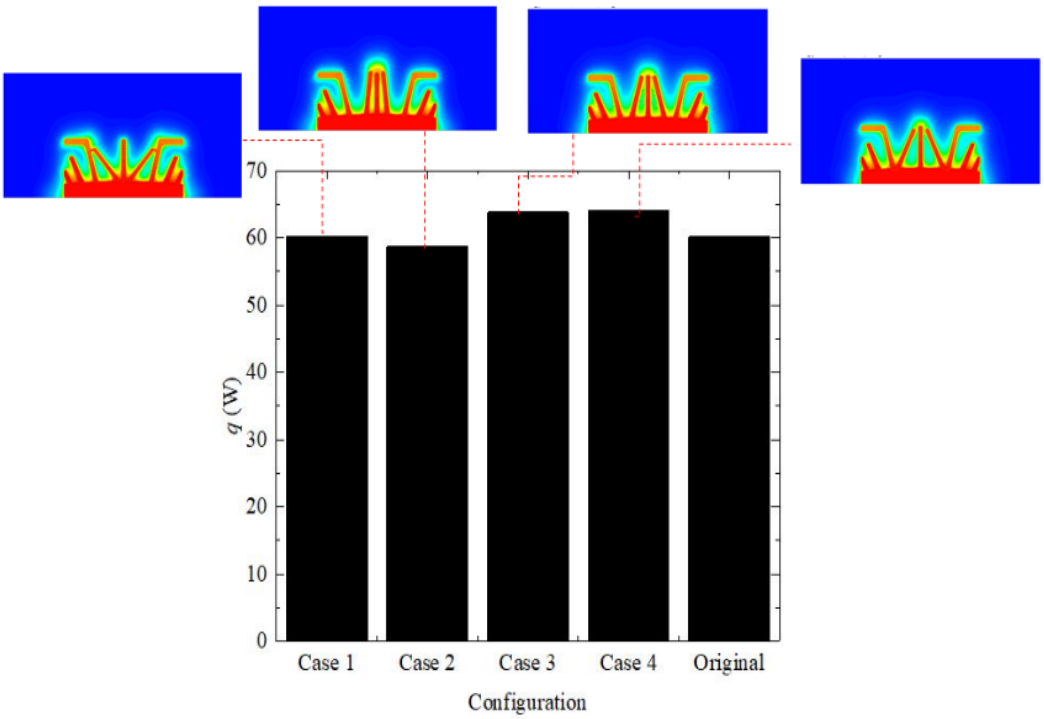

Figure 8. Thermal performance of five different heat sinks studied and thermal fields for the new proposed configurations.

7. ACKNOWLEDGEMENTS

T.M. Claudino thanks CNPq (National Counsel of Technological and Scientific Development – Brasília, DF, Brazil) for scientific initiation scholarship. L. A. Isoldi, L.A.O. Rocha, P. L. J. Drews Júnior and E.D. dos Santos thank CNPq for research grants (Process: 309648/2021-1, 307791/2019-0, 309069/2022-0, and 308396/2021-9).

8. REFERENCES

ANSYS FLUENT 2021 R1 —FLUENT user's guide, ANSYS Inc, 2021.

Bejan, A., 2013. *Convection heat transfer*, John Wiley & Sons, New York, USA.

Bejan, A. 2000. *Shape and structure, from engineering to nature*, Cambridge University Press, New York, USA.

Chung, Y., Kim, M.S., 2019. Thermal analysis and pack level design of battery thermal management system with liquid cooling for electric vehicles, Energy Conversion and Management, Vol. 196, pp. 105 – 116. https://doi.org/10.1016/j.enconman.2019.05.083

Drews, P.L., Neto, A.A., Campos, M.F.M., 2014, "Hybrid unmanned aerial underwater vehicle: modeling and simulation". In *Proceedings of IEEE/ESJ International Conference on Intelligent Robots and Systems*, Chicago, USA, pp. 4637 – 4642. ISSN 2153-0858.

Dos Santos, E.D., Isoldi, L.A., Gomes, M.N., Rocha, L.A.O., 2017. "The constructal design applied to renewable energy systems". In: Rincón-Medía, E., de las Heras, A. (eds.). *Sustainable Energy Technologies*, 1 Ed., Boca Raton: CRC Press, Taylor & Francis Group, 63 – 87.

Grando, R.B., Pinheiro, P.P., Bortoluzzi, N.P., Da Silva, C.B., Zauk, O.F., Pineiro, M.O., Aoki, V.M., Kelbouscas, A.L.S., Lima, Y.B. Drews-Jr, P.L.J., Neto, A.A., 2020, "Visual-based autonomous unmanned aerial vehicle for inspection in

indoor environments". In *Proceedings of the 2020 Latin American Robotics Symposium (LARS), 2020 Brazilian Symposium on Robotics (SBR) and 2020 Workshop on Robotics in Education (WRE)*, Natal, Brazil. https://doi.org/10.1109/LARS/SBR/WRE51543.2020.9307024

Han, D.W., Özisik, M.N., 1993, *Heat conduction*, John Wiley & Sons, 2nd Edition, New Jersey, USA.

Hilpert, R., 1933, *Wärmeabgabe von beheizten Drähten und Rohren im Luftstrom, Forsch. Ingenieurwesen*, Vol. 4, pp. 215–224.

Horn, A.C., 2019. *Robôs híbridos: ar-água: um veículo não tripulado do tipo quadricóptero com foco na eficiência energética*. MSc. Thesis, Graduate Program of Computation, Federal University of Rio Grande, Rio Grande, Brasil.

Igarashi, T., 1985, Heat transfer from a square prism to an air stream, International Journal of Heat and Mass Transfer, Vol. 28, pp. 175–181. https://doi.org/10.1016/0017-9310(85)90019-5

Incropera, F.P., Dewitt, D.P., Bergman, T.L., Lavine, A.S., 2008, *Fundamentos de transferência de calor e de massa*, LTC, 6ª ed., Rio de Janeiro, RJ, Brasil.

Launder, B.E., Spalding, D.B., 1972, *Lectures in mathematical models of turbulence*, Academic Press, London.

Maliska, C.R., 2004, *Transferência de calor e mecânica dos fluidos computacional*, Livros Técnicos e Científicos Editora S. A., Rio de Janeiro.

Menter, F.R., 1993, Zonal two equation κ-ω turbulence models for aerodynamic flows, In *Proceeding of AIAA 24th Fluid Dynamics Conference*, AIAA 93-2906, Ames Research Center, Moffett Field, USA.

Menter, F.R., Kuntz, M., and Langtry, R., 2003, Ten years of industrial experience with the SST turbulence model, *Turbulence, Heat and Mass Transfer*, Vol. 4, pp. 625–632.

Naqiuddin, N.H., Saw, L.H., Yew, M.C., Yusof, F., Ng, T.C., Yew, M.K., 2018, Overview of micro-channel design for high heat flux application, Renewable and Sustainable Energy Reviews, Vol. 82, pp. 901-914. https://doi.org/10.1016/j.rser.2017.09.110.

Patankar, S.V., 1980. *Numerical heat transfer and fluid flow*, McGraw Hill, New York, USA.

Patankar, S.V., Spalding, D.B., 1972, A calculation procedure for heat, mass and momentum transfer in three-dimensional parabolic flows, International Journal of Heat and Mass Transfer, Vol. 15, pp. 1787 – 1806.

Pope, S.B., 2008. *Turbulent flows*, Cambridge University Press, New York, USA.

Ranjan, P., Dewan, A., 2015, Partially averaged Navier Stokes simulation of turbulent heat transfer from a square cylinder, International Journal of Heat and Mass Transfer, Vol. 89, pp. 251–266. https://doi.org/10.1016/j.ijheatmasstransfer.2015.05.029

Teixeira, F.B., Lorenzini, G., Errera, M.R., Rocha, L.A.O., Isoldi, L.A., Dos Santos, E.D., 2018, Constructal design of triangular arrangements of square bluff bodies under forced convective turbulent flows, International Journal of Heat and Mass Transfer, Vol. 126, pp. 521–535. https://doi.org/10.1016/j.ijheatmasstransfer.2018.04.134.

Versteeg, H.K. and Malalasekera, W., 2007. *An introduction to computational fluid dynamics: the finite volume method*, Pearson Education Limited, Harlow, England.

Wilcox, D.C., 2006, *Turbulence modeling for CFD*, 3d ed., DCW Industries, La Canada, USA.

Yao, H., Qin, R., Chen, X., 2019, Unmanned aerial vehicle for remote sensing applications — A review, remote sensing, Vol. 11(12), 1443. https://doi.org/10.3390/rs11121443.

Zauk, O.F., 2022. *Estudo numérico e design construtal empregados para investigar a configuração geométrica do dissipador de uma jetson nano para o resfriamento de um drone autônomo*, Conclusion Undergraduate Course Work in Mechanical Engineering, Federal University of Rio Grande, Brasil.

9. RESPONSIBILITY NOTICE

The author(s) is (are) the only responsible for the printed material included in this paper.